Micro-opto-electro-mechanical devices and on-chip optical processing

M. Edward Motamedi, MEMBER SPIE
Rockwell Science Center
1049 Camino Dos Rios
Thousand Oaks, California 91360
E-mail: motamedi@scimail.risc.rockwell.com

Ming C. Wu
University of California, Los Angeles
Electrical Engineering
405 Hilgard Avenue
Los Angeles, California 90095

Kristofer S. J. Pister
University of California, Berkeley
Electrical Engineering and Computer Sciences
491 Cory Hall
Berkeley, California 94720

Abstract. Micro-optical components, such as diffractive and refractive microlenses, micromirrors, beamsplitters, and beam combiners, have recently received considerable attention in the optics R&D centers and finally in the manufacturing community. This achievement is due to micro-electro-mechanical (MEM) technology that has demonstrated major improvements in overall performance and cost of optical systems while offering the possibility of relativity rapid transition to products for military, industrial, and consumer markets. Because of these technology advances, an industrial infrastructure is rapidly becoming established to combine micro-optical components and MEM-based microactuators for on-chip optical processing. Optical systems that once were considered to be impractical due to the limitations of bulk optics can now easily be designed and fabricated with all required optical paths, signal conditioning, and electronic controls integrated on a single chip. On-chip optical processing will enhance the performance of devices such as focal-plane optical concentrators, smart actuators, color separators, beam shapers, fiber data distribution interface (FDDI) switches, digital micromirror devices (DMDs), and miniature optical scanners. We review advances in microoptical components developed at the Rockwell Science Center. We also review the potential of on-chip optical processing and the recent achievement of free-space integrated optics and micro-optical bench components developed at UCLA, and DMDs developed at Texas Instruments.
[S0091-3286(97)01105-7]

Subject terms: micro-opto-electro-mechanical systems; micro-optics; actuators; integration; mirrors; microlens; digital micromirror devices (DMDs); fiber data distribution interface (FDDI); digital video.

Paper MEM-12 received Nov. 14, 1996; revised manuscript received Dec. 20, 1996; accepted for publication Jan. 15, 1997.

1 Introduction

Micro-optical components, such as diffractive and refractive microlenses, have recently received considerable attention for the development of optical systems.[1–5] Achievements in micro-optical functions such as focal-plane optical concentration,[1,2,6] optical-efficiency enhancement, digital video development, color separation, and beam shaping and transforming[7] have demonstrated the potential of this technology. In the first generation of the miniaturized optical system, micro-optical components were hybridized with electronic circuits and in some cases with movable components such as scanning mirrors and piezoactuators. As microelectronic technology advanced by novel development in micromachining and micro-electro-mechanical (MEM) technology, miniaturized optical systems also advanced to nearly complete monolithic systems.

MEM technology combines mechanical structures with electronics to perform mechanical motions, offering a host of actuators and wide applications in optical systems. Merging micro-optics, microelectronics, and micromechanics creates a new and broader class of micro-opto-electro-mechanical (MOEM) devices,[8,9] which may attract additional industrial demonstrations of commercial devices. A few examples are torsional mirrors, digital micromirror devices (DMDs), laser scanners, fiber data distribution interface (FDDI) switches, 3-D tunable Fabry-Perot etalons, optical shutters, MEM optical switches, optical interconnections, data storage devices, and MEM corner cube reflectors. Integrated devices based on MOEM systems can form free-space integrated optics and consequently push technology to the development of a micro-optical bench on a chip.

In this paper, we first review recent developments and achievement in micro-optics (Sec. 2) and in micro-optical MEM and on-chip optical processing (Sec. 3). In Sec. 3, we discuss the development of the micro-optical bench and free-space interconnections.[10–14] Then we introduce several applications of optical MEM devices with the potential of on-chip optical processing (Sec. 4). We discuss in detail the development of a 3-D tunable Fabry-Perot,[15–19] an FDDI optical bypass switch,[20–22] a MEM corner cube reflector,[23] a digital display using DMDs,[24–29] and, finally, optical scanners.[30]

2 Micro-optics

Micro-optics technology is becoming increasingly essential to the development of many dual-use optical systems. Optical components such as diffractive and refractive

microlenses,[1–5] multilevel optical gratings, beamsplitters, and optical transformers[7] are being incorporated into advanced military sensor systems and commercial products. Micro-optics is an enabling technology for applications that cannot be addressed using conventional optics. In the following we discuss some of these microcomponents as subtechnologies of micro-optics.

2.1 *Diffractive Microlenses*

The first breakthrough in optical processing was the development of diffractive microlenses. A diffractive microlens is a micro-optical component as small as a few tens of microns in diameter and with a thickness on the order of an optical wavelength. Its speed can be as fast as f/0.3 in air for high-index materials such as silicon and GaAs,[1] and about f/1 for quartz and glass substrates. A diffractive microlens is an approximation of a kinoform, or continuous diffractive lens, designed by applying a phase-function constraint between 0 and 2π to subtract an integral number of wavelengths from the lens transmittance function. Theoretically, a kinoform lens has a 100% diffraction efficiency. The kinoform lens structure can be approximated by multilevel lithography and stepwise etching. To fabricate a multistep process, binary-optical design is considered. Binary optics will reduce the number of lithographic masks by a factor of $2^m/m$, where m is the number of required masks.

For a binary-optics structure, the phase transmittance is quantized with the phase step heights defined by the relation

$$d(m)=\frac{\lambda}{(n-1)2^m}, \tag{1}$$

where λ is the light wavelength in free space, n is the index of refraction of the lens material, m is the mask number for the level-m process, and $d(m)$ is the etch depth of the level m. An m-mask process produces an $M=2^m$-step approximation to a continuous blazed diffractive structure. The efficiency of the incident energy diffracted into the first order is given by

$$\eta=\left[\frac{\sin(\pi/M)}{\pi/M}\right]^2. \tag{2}$$

For $M = 4, 8$, or 16 we have $\eta = 0.81, 0.95$, or 0.99, respectively.

Since microlenses operate over a small range in incident angle, a simple planar thin-film lens design is acceptable. The optical path difference (OPD) function for each lens is used to derive the following relationship among the zone radius, focal length, and wavelength[2]:

$$r(p,m)=\left[\left(\frac{p\lambda}{n\,2^m}\right)^2+2f\left(\frac{p\lambda}{n\,2^m}\right)\right]^{1/2}, \tag{3}$$

where f is the focal length, $p=0, 1, 2, 3...$, n is the refractive of the substrate, and $r(p, m)$ gives the successive zone radii for the patterns in mask number m.

Figure 1 shows a processing cycle for fabrication of an eight-level binary-optics microlens. Figures 1(a), 1(b), and 1(c) illustrate the process of two-phase, four-phase, and eight-phase microlenses where the etch depth and zone radii of each process can be determined from Eqs. (1) and (3) for $m = 1, 2$ and 3, respectively.

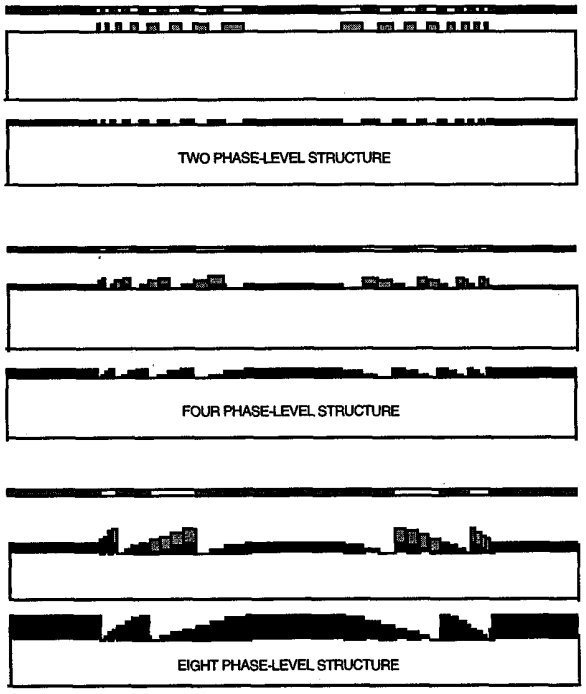

Fig. 1 Processing cycle of an eight-phase-level binary-optics microlens.

Binary optics can produce microlenses and lens arrays with submicron features, located and packed precisely together, with an accuracy of a fraction of a micron. Binary-optics microlenses with multilevel relief structures can produce diffraction efficiencies higher than 90%, which enables design of many complex optical systems not possible with bulk optics. Recently, this technology has demonstrated high-quality microlens arrays, which have attracted many applications in both passive and active optical sensors.[1,2]

Three independent optical and processing parameters that are important in the design of a binary-optical microlens are the wavelength λ, the f number (F), and the smallest process feature size or critical dimension, CD. The value of F is equal to f/d, where f is the focal length and d is the microlens diameter. For a typical eight-phase-level binary-optic microlens the CD value is

$$\mathrm{CD}=\lambda F/4. \tag{4}$$

In most production laboratories the minimum VLSI feature size is 0.5 to 1 μm. This limits the binary optic microlens speed to between f/6 and f/3 for wavelengths from 0.632 μm (HeNe laser) to 0.850 μm (typical laser diode), respectively. Figure 2 shows an f/6 quartz microlens array designed for $\lambda = 0.632$ μm with microlens diameter 200 μm and 100% fill factor.

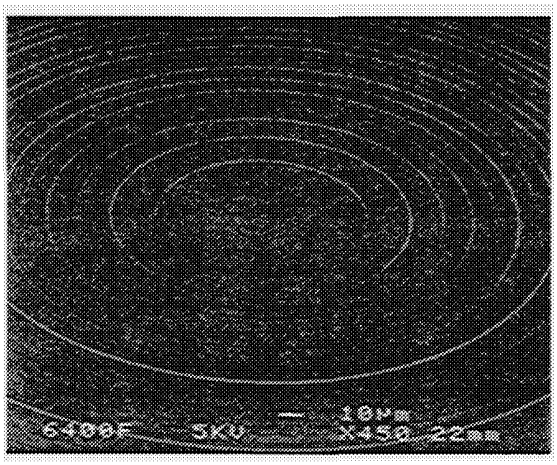

Fig. 2 SEM microphotograph of a center zone of an f/6 quartz microlens designed for $\lambda = 0.632$ μm with microlens diameter of 200 μm and 100% fill factor.

According to Eq. (4), higher-speed (lower F) microlenses can be fabricated for infrared applications. Figure 3 shows an SEM view of an f/0.6 microlens designed for 1–10 μm with microlens diameter 240 μm and 100% fill factor.

An important consideration for diffractive microlenses is the diffraction efficiency. The efficiency with which the light is diffracted to the first-order focus increases with the number of phase levels [see Eq. (2)]. In practice, the efficiency is reduced by a number of processing factors. Values of 90% have been achieved for eight-phase-level microlenses. The extent to which this is acceptable will depend on the application.

A major feature of diffractive microlenses is the planar nature of the structure. The surface relief is on the order of the design wavelength. This will reduce the volume and weight of the optics in a typical system relative to an all-refractive design. Diffractive optical devices can be made either directly in the substrate by reactive-ion etching (RIE),[1,2] or on the surface by thin-film deposition and lift-off techniques.[3,6]

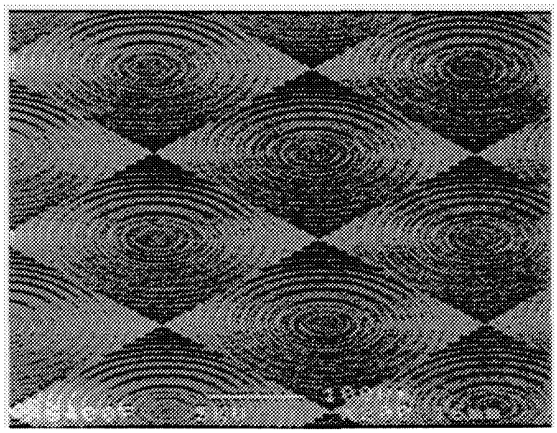

Fig. 3 SEM view of an f/0.6 microlens designed for 1 to 10 μm with microlens diameter of 240 μm and 100% fill factor.

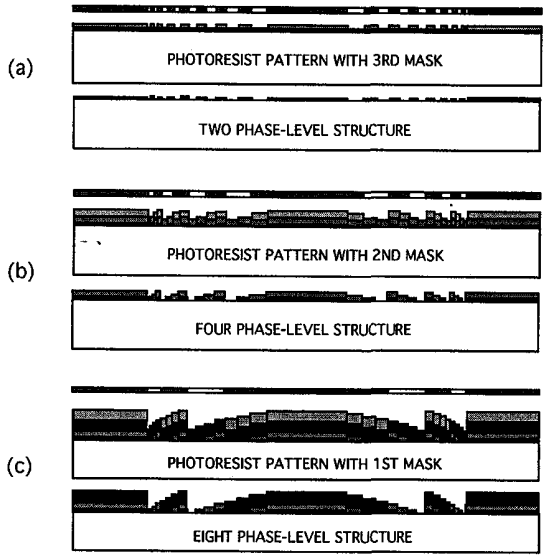

Fig. 4 A typical profile of an eight-level thin-film binary-optics microlens processed by projection lithography.

The advantage of using thin-film deposition to fabricate binary-optics microlenses is the finer control that can be applied to film thickness than to etch depth in the RIE process. This will increase the diffraction efficiency of the device, assuming all the other process parameters remain unchanged. A further advantage of thin-film deposition is the ability to generate microlenses using materials that are not easily processed by RIE.[3]

The design considerations for deposited microlenses are identical to those used for RIE-processed microlenses. Identical mask sets can be used for both processes. Motamedi et al. have demonstrated a single-material deposition and liftoff method.[3] This work also emphasizes submicrometer process and technology trade-offs between standard RIE and thin-film deposited binary-optics microlens arrays. The process steps of the thin-film deposition method are shown in Fig. 4.

One approach to this process is to use an image-reversal photoresist, which has the advantage of producing a negative slope pattern, a crucial requirement for submicron lift-off processing. An example of the use of the thin-film method to generate microlenses in a material that is not readily processed using RIE is an all-sapphire (Al_2O_3) microlens array. Figure 5 is a SEM photomicrograph of an eight-phase level f/17 thin-film microlens. The optical quality of these microlenses was evaluated by measuring the point spread function.[3]

The spectral range of shortwave infrared (SWIR) focal-plane arrays (FPAs) is from 1.5 to 2.5 μm. These arrays have numerous applications in medicine, security, industrial inspection, and IR astronomy, all of which will benefit from diffractive optics. High sensitivity at high operating temperature is often important in these applications. Conventional FPAs have relatively poor sensitivity and low signal-to-noise ratio at high temperatures. Integrating binary-optics microlenses and hybrid FPA technologies leads to a new approach to reducing detector size while

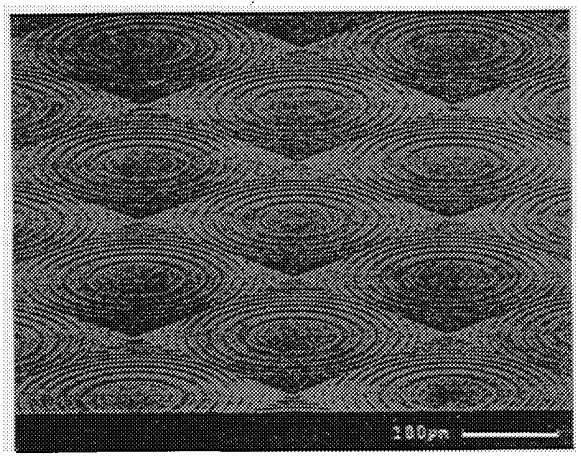

Fig. 5 Photomicrograph of a completed f/17 sapphire thin-film binary-optics microlens using image-reversal lithography. The microlens has eight phase levels and a speed of f/12 at the corners.

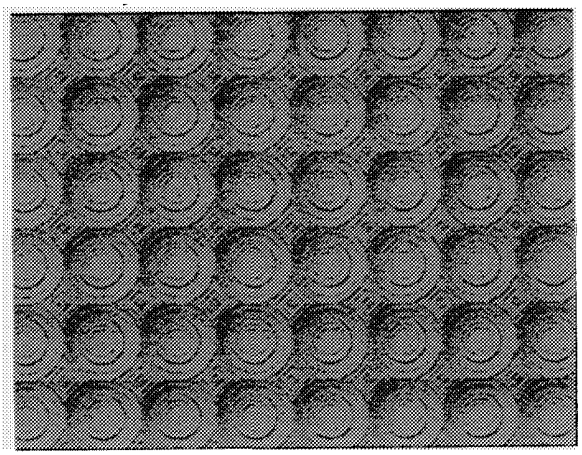

Fig. 7 A portion of a 16-phase thin-film microlens array processed at Rockwell.

retaining a given image resolution and optical collection area. The resultant detector volume reduction has led to a significant decrease in detector dark current and hence to an increase in device performance.

Recent results from Rockwell[6] show that integration of micro-optics and SWIR HgCdTe can produce detectors that perform exceptionally at elevated operating temperatures. The detector configuration of this effort is shown in Fig. 6. Here light incident on the back side of the substrate is focused by a thin-film binary optic into the detector, leading to total internal reflection; the mesa sides augment the diodes light-gathering abilities beyond the physical extent of the active layer. Note that with no buffer layer, delineation of the active area is incomplete, and the effective optical area of the detector will be wavelength-dependent due to shorter wavelengths being more effectively absorbed by the mesa valleys, which have larger area. Retaining the planar geometry on top of the mesa preserves the passivation advantage of the cap layer and as a result enhances the optical efficiency of the system.

Photolithography of these microlenses is done by a GCA 5X I-line stepper. The projection system requires alignment mark fiducials for mask-level-to-mask-level alignment on the stepper. The fiducials used by the stepper are processed first, using a Karl Suss back-side aligner with IR/visible light source for alignment. The Karl Suss uses an infrared light source to view circuit-side fiducials through the substrate. Figure 7 shows a portion of a thin-film 16-phase binary-optics microlens array processed by the above technique.

The readout devices used in this work were simple stripline fanouts made on sapphire substrates. Hybridization was accomplished in the traditional method using cold-welded In bumps. This same technique is used for making fully multiplexed FPAs. A complete test sample consisted of a 5 × 5-mm HgCdTe pattern that contained a 4 × 64 array of devices of varying types on 48-μm centers. A typical package of FPAs and integrated microlenses is shown in Fig. 8.

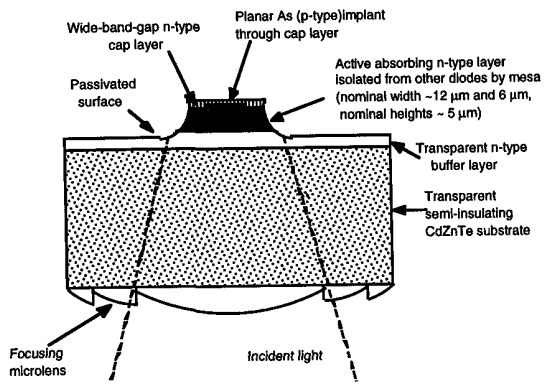

Fig. 6 Planar mesa architecture, demonstrating the potential for integration of microlens with FPA.

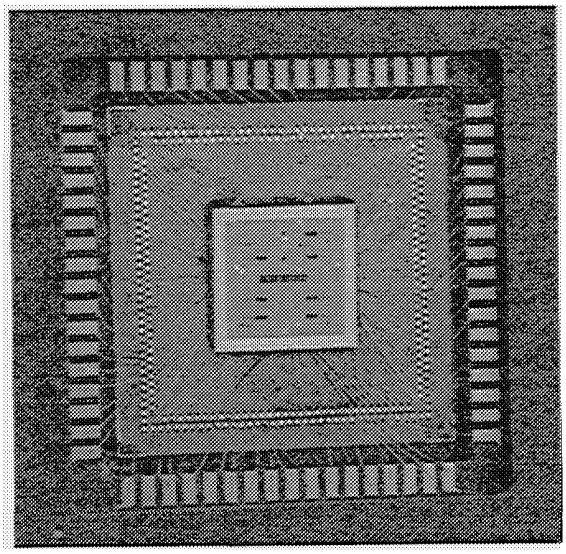

Fig. 8 A typical complete package for monolithic integration of FPAs and diffractive optics.

2.2 *Refractive Microlenses*

Refractive microlenses may provide an attractive, low-cost alternative to diffractive microlenses. Refractive and diffractive microlenses are complementary, and in some cases refractive optics is the sole means of optical system design. For example, in the case of a short-wavelength optical system ($\lambda < 1\ \mu$m) requiring high-speed microlenses ($<$f/4), diffractive optics faces a process limitation (CD$<1\ \mu$m).[2]

Refractive microlenses and microlens arrays have been fabricated by forming photoresist cylinders, and then heating until the resist melts and flows, forming a refractive lens profile. Where submicrometer tolerances are required for coherent optical performance, process control of photoresist patterning is crucial for optimum lens quality with minimum aberration. Process issues include initial substrate cleaning, humidity control, careful choice of photoresist, and precise control of temperature and duration of the melt process.

For applications where photoresist microlenses are incompatible with the operating environment, refractive microlenses can be generated in a suitable material by first generating photoresist microlenses, then reflowing under temperature treatment to form spherical shapes[4] and transferring this pattern into a solid material such as silicon, GaAs, or fused silica by either reactive-ion etching[4] or ion milling.[5] Successful microlens fabrication requires accurate control of etching and photoresist lithography processes. The fabrication issues are spatial uniformity, reproducibility and control of photoresist microlens diameter, sag and shape, reproducibility of reactive-ion etch rate and selectivity, and surface roughness. Many of these issues are interrelated. The final microlens shape and dimensions depend both on the photoresist processing and on the reactive-ion etch conditions. Thus, any variations in the photoresist lens shape may be corrected in the subsequent etch phase if the dependence of the etch behavior on process conditions (pressure, power, gas composition) is accurately known.

In the reactive-ion etch pattern transfer process, the relative etch rates of the photoresist mask material and solid material can be controlled, mainly by the reactive gas mixture. For fused-silica microlenses, both carbon- and fluorine-bearing species are needed to etch silica-containing materials, while fluorine- and oxygen-bearing species etch the photoresist. The gas species, pressure, temperature, and rf power dependence of the etch selectivity and rates need to be determined for the RIE system used in the fabrication and for the solid microlens material. The microlens arrays are usually characterized by SEM, surface profilometry, and interferometric microscopy. The profilometric data are curves-fitted to extract the conic coefficients. For a more detailed discussion of photoresist microlens processing, conditions to achieve uniform and dimensionally accurate refractive microlens and methods of characterization, refer to Refs. 4 and 5. In the following we will summarize some Rockwell achievements in process development, and present some design issues.

2.2.1 *Process development*

Our goal has been to develop a simple process to reproducibly fabricate microlens arrays that satisfy a wide range of characteristics. Modeling studies indicated that in the pattern transfer process, photoresist lens sags close (within 10%) to the desired sag in the solid material are necessary for faithful reproduction of the spherical surface. In practice, the resist microlens sag usually differs substantially from the sag of the microlens in the etched material, due to limitations on the photoresist thickness imposed by the fabrication requirements. We could successfully fabricate photoresist microlenses when their aspect ratios (height-to-diameter ratios) were in the range of 3% to 10%. Low-aspect-ratio ($<3\%$) resist islands did not develop into convex surfaces even at the highest anneal temperatures. High-aspect-ratio ($>10\%$) islands reflowed into spherical shapes but also spread to larger diameters, severely compromising the quality of closely spaced microlenses. Within this range, formation temperature increased with decreasing aspect ratio, so that low-aspect-ratio levels generally required temperatures close to 200°C. Substrate type and surface preparation were critical in controlling reflowing of the photoresist.

The photoresist thickness depends on the resist viscosity, spin rate, and spin time. For good uniformity, spin rates and times need to be maintained within certain limits, which restrict the range of thicknesses, and hence resist lens sags, obtainable for a given type of resist. Large-diameter, low-F lenses require thick ($>15\ \mu$m) lenses using photoresist layers. Photolithograpic processing of these lenses was difficult, and generally did not result in good lenses, especially for closely spaced arrays. Therefore, we preferred to fabricate thinner ($<15\ \mu$m) lenses using photoresist and to produce thicker solid material lenses via the etch process. Because of this and the limitations on the aspect ratios discussed above, for a given lens diameter, there appears to be an optimum range of resist thicknesses that result in good lenses with accurate dimensions. For all of the above reasons, photoresist microlenses generally differ in sag from the sag of the solid lenses and therefore require reactive ion etching with carefully controlled etch selectivity to achieve the solid lens dimensions and surface profiles desired.

2.2.2 *Design issues*

At Rockwell, we have designed and fabricated refractive microlenses by RIE and ion milling in fused quartz, bulk silicon, CdTe, GaAs, InP, and GaP; and by thin film deposition of Ge films on fused silica and Al_2O_3. Lens diameters ranged from 30 to 500 μm, and lens f numbers were in the range of f/0.76 to f/6. In the calculation of the lens power, the thick lens formula was used.

$$F = \frac{1}{2z\{n(1-z^2)-[1-(nz)^2]\}}, \tag{5}$$

where n is the refractive index, and $z = a/r$ with a the lens radius and r the radius of curvature. This is exact and should be used especially for high-speed microlenses (low f numbers).

Reliable and reproducible fabrication of microlens arrays depends on accurate control of photolithographic and reactive-ion etching processes. Photoresist microlenses can be reliably fabricated within a range of aspect ratios. Di-

Fig. 9 SEM micrograph of an f/4.2, 200-μm-diam closely spaced microlens array fabricated in fused silica.

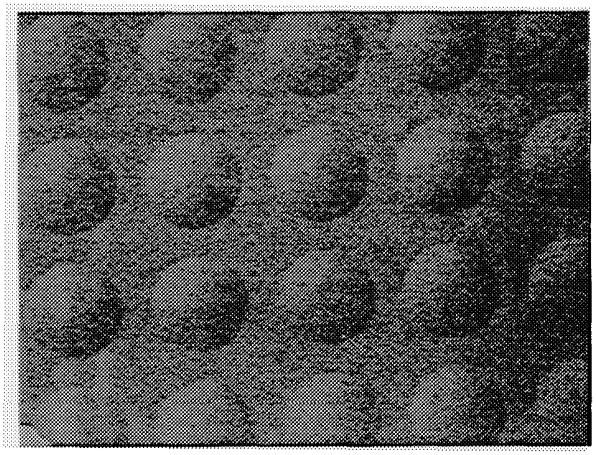

Fig. 11 SEM micrograph of an f/1, 50-μm-diam linear microlens array fabricated in InP.

mensional control of microlenses in the solid material can then be tailored by carefully controlled reactive-ion etching. Both mixtures of SF_6 and of O_2 with CF_3H were used to accurately control the lens sag during etching.

2.2.3 *Typical refractive microlens processed at Rockwell*

Rockwell has developed automated processes for both reactive-ion etching and reactive-ion milling to fabricate refractive microlenses with any tight performance requirement. These processes can easily control the microlens shape and conic coefficient to remove the spherical aberration created by the photoresist reflow method.

Figure 9 is a SEM micrograph of a closely spaced microlens array. To limit the aperture to the actual lenses, the flat areas of the substrate between the microlenses were coated with a photolithographically defined layer of evaporated chrome. Figure 10 is a SEM micrograph of a linear array of very fast fused silica microlens with f number 0.86, 80-μm diam, and centers spaced at 100 μm. Figure 11 is a SEM micrograph of an InP microlens with speed f/1, 50-μm diam, and centers spaced at 70 μm. Figure 12 is a SEM micrograph of a square Ge microlens array with speed f/2, 50-μm side, and centers spaced at 60 μm.

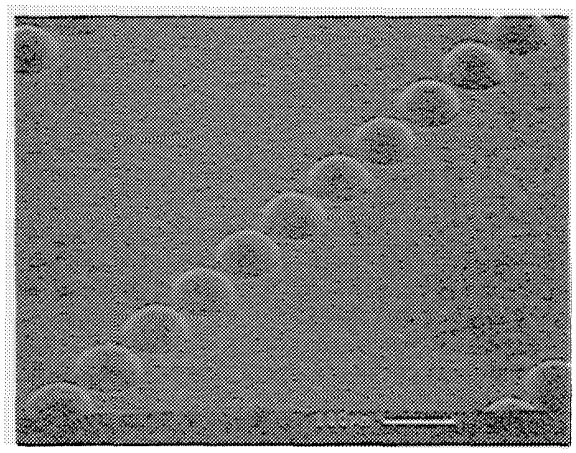

Fig. 10 SEM micrograph of an f/0.86, 80-μm-diam linear microlens array fabricated in fused silica.

3 Micro-optical MEMs: MOEM Systems

Microfabrication technology has been developed for integrated circuits and microchips during the past two decades. Remarkable progress in sculpting and micromachining has added a third dimension to integrated circuits; as a result, a 3-D microstructure can be fabricated. To make micromachined devices dynamic, mechanical motions are combined with electronic circuits to create a new technology called the micro-electro-mechanical systems (MEMS). Recent advances in MEMs have produced novel subsystems, containing completely assembled motors, valves, and pumps, all fractions of a millimeter in size.

MEM structures can be generated by either bulk or surface micromachining processes. In bulk miromachining, structures are sculpted directly into the bulk substrate, creating 3-D features. The substrate is etched using either chemical or dry etching. Processing can occur on one or both sides of the water, the latter requiring back-to-front wafer alignment. In some cases the MEM structure can be formed in the substrate surface without sculpting the substrate itself. A sacrificial layer is usually used, acting as a temporary platform, to be etched away after the rest of the

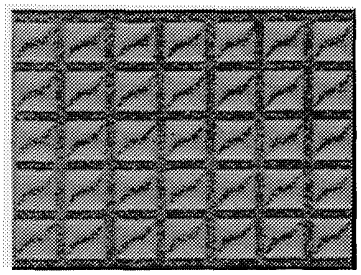

Fig. 12 SEM micrograph of an f/2, 50-μm-square microlens array fabricated in Ge.

MEM structure has been defined. This type of process is referred to as surface micromachining. The sacrificial layer material must be selected to provide good etch selectivity relative to the other device materials.

In the following we discuss major novelties of MEMS. We then introduce examples of the devices that require both MEMS and micro-optic technologies. This class of devices (MOEM systems) will be discussed to explain on-chip optical processing.

3.1 *Microsensors and Microactuators*

Microsensors and microactuators are subtechnologies under MEMs that recently have experienced significant advances in device design, fabrication, materials, testing, packaging, and applications. Some demanding applications of these technologies are micromotors and articulated microstructures. More ambitious applications could include actuators in a range of electromechanical systems.

A fascinating range of micromechanical sensors and actuators that could be inexpensively mass-produced using silicon micromachining and integrated circuit (IC) fabrication techniques is now envisioned. Many interesting demonstrations of MEM sensors, motors, and actuators that highlight the phenomenal possibilities for this emerging technology have been made recently. Considerable industrial attention is now being directed at MEM technology to develop applications, assisted by the impressive related capabilities that have been developed at a number of U.S. research centers.

The application of MEM technology is very much focused on the design and development of microsensor and microactuator devices. These devices have at least one dimension that is on the order of micrometers and are not more than several millimeters in all the remaining dimensions. Microsensors are important elements of smart machines. They contribute much to reducing the overall system size and weight, and consequently, the cost.

Microsensors/microactuators based on MEM technology have inherently a monolithic integration capability that not only reduces the device size by one order of magnitude but also tremendously improves their performance. One example of such a device is the micromachined active probe designed and developed at University of Michigan for neural information processing studies. The device has 10 channels with on-chip signal processing. Figure 13 shows a photograph of this probe where the tip of the probe is passing through the eye of a needle.

3.2 *MOEM Systems and On-Chip Optical Processing*

Both MEM and micro-optic technologies have one critically important common feature: both technologies are compatible with IC processing. This feature ensures that the final device can be batch-processed at low cost. The standard IC process is generally confined to the surface of the wafer (Si or GaAs), extending only a few microns into the bulk. IC processes tailored to precisely control the etch depth and sidewalls with dimensions far inside the bulk lead to what is termed a three-dimensional integrated circuit or, more commonly, micromachined circuit. Micromachining is also a common process requirement for both micro-optic and MEM technologies. The overlapping of

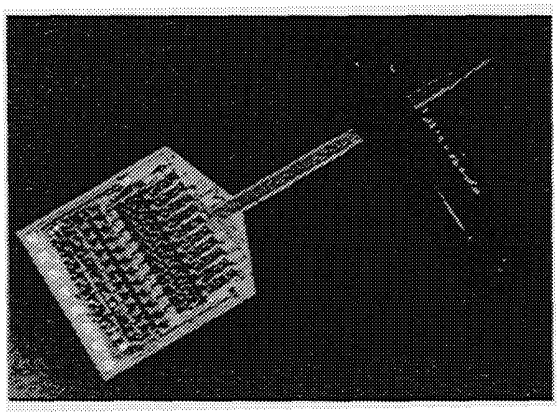

Fig. 13 Ten-channel MEM probe for recording neurons, developed by University of Michigan.

three major fields—electronics, mechanics, and optics, represented in the merging of micro-optics and micromechanics (MOEM systems)—is required for successful integrated optical processing. We now discuss devices that represent MOEM systems and that are candidates for on-chip optical processing.

In the past several years, researchers have proposed and demonstrated many applications of MOEM systems. Most of these demonstrations were based on miniaturized systems with micro-optics and micromechanics, where fabrication of all the optical and MEM components on a single chip was not necessary.

The recent development at UCLA of surface micromachined microhinge and free-space integrated optics[10–14] resulted in a micro-optical bench that has attracted much attention for optical processing on-chip. Free-space integrated optics offers many advantages over the guided-wave approach: high spatial bandwidth (diffraction-limited), noninterfering optical routing, three-dimensional optical interconnection, and optical signal-processing capability (e.g., Fourier optics). However, it is more difficult to integrate free-space optics on a single substrate, since most monolithically fabricated free-space optical elements lie on the surface of the substrate.

Micromachining of silicon substrates has been applied to integrated optics and the realization of a miniature optical bench. Also, surface micromachined hinges and spring latches[10] have been used to achieve monolithic fabrication of three-dimensional micro-optics.[13] This technology opens a new area for integrated optics in free space. Using this new technique, thee-dimensional micro-optical components can be fabricated integrally on a single Si chip. The Si substrate serves as a micro-optical bench on which microlenses, mirrors, gratings, and other optical components are prealigned in the mask layout stage using computer-aided design and then constructed by microfabrication. Additional fine adjustment can be achieved by on-chip microactuators and micropositioners, such as rotational and translational stages. With hybrid integration of active optical devices, a complete optical system can be constructed, as illustrated in Fig. 14.

The three-dimensional micro-optical system is constructed on a Si substrate by the surface micromachining

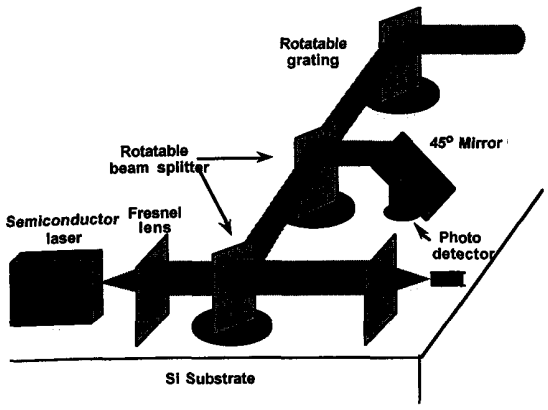

Fig. 14 The schematic diagram illustrating the micromachined free-space micro-optical system on a single Si chip.

technique. In the following, we discuss some of the major components of a typical optical train required for on-chip optical processing.

3.2.1 *Microbase, micromount, and microhinge design*

The micro-optics plates used for mirror, beamsplitter, microlens array, grating, and collimator are processed by surface micromachining, and they are released from the substrate by selectively removing the sacrificial material (deposited SiO_2) using hydrofluoric acid after fabrication. After the release etching, the poly plates with micro-optics patterns are free to rotate around hinge pins (Fig. 15).

When the plate is lifted up, the top portion of the spring latch slides into a slot on the plate and snaps into a narrower part of the slot, thus preventing further motion of the plates. The torsion spring connecting the spring latch to the substrate creates the spring force, which tends to force the spring latch back to the substrate, thereby locking the plate in its place. The length of the spring latch fixes the angle between the plate and the substrate. After the three-dimensional micro-optical element is assembled, a layer of gold is coated on the lifted poly surfaces. In binary-amplitude Fresnel-zone plates or micromirrors, a thick

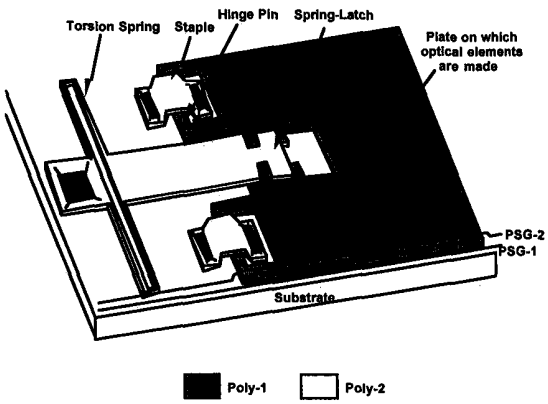

Fig. 15 The schematic structure of MEM micro-optical elements before assembly.

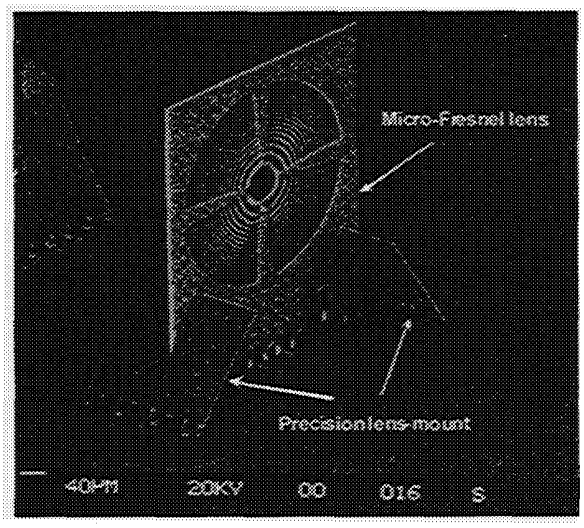

Fig. 16 SEM photograph of a Fresnel microlens with precision lens mount.

layer of gold is needed to completely block the light passing through the dark zones or to make a perfectly reflecting mirror. On the other hand, thinner gold is needed for partially transmitting mirrors or beamsplitters.

3.2.2 *Fresnel microlenses*

Figure 16 shows a SEM photograph of a three-dimensional Fresnel microlens after assembly. The diameter of this lens is 280 μm, with a designed optical axis of 254 μm for passive integration of an edge-emitting semiconductor laser. Because of the height of the lens plate, the angles between the lens plates and the substrate have some variations even though they are coarsely defined by the spring latches. Such variations are not tolerable in large optical systems. Therefore, an additional *lens mount* is designed to precisely define the angles of the three-dimensional micro-optical elements. The lens mount consists of two folded polysilicon plates, which are fabricated integrally with the microlens. It has a V-shaped opening at the top to guide the lens plate into a 2-μm-wide groove in the center. It can be made as tall as the lens itself; therefore, the angle defined by the lens mount is much more precise. The lens mount also greatly improves the mechanical strength and stability of the micro-optical elements.

The optical performance of the three-dimensional Fresnel microlens has been tested by collimating a divergent beam emitted from a single-mode fiber at $\lambda = 1.3$ μm. The intensity FWHM divergence angle is reduced from 5.0 to 0.33 deg by the lens. The collimated beam profile fits the Gaussian shape very well (95% fit).

3.2.3 *Translation stage*

One unique feature of implementing a micro-optical bench using surface micromachining is that micropositioners and microactuators can be monolithically integrated in the same fabrication processes for different types of optical translators. This allows the alignment of the optical systems to be fine-adjusted, in addition to the coarse alignment done at the design stage using CAD layout tools. Using similar

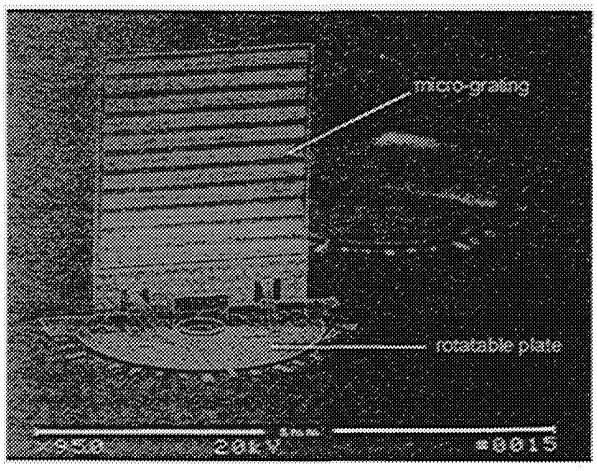

Fig. 17 The diffraction grating integrated with a rotational stage.

structures as the micromotors, rotational stages and linear micropositioners can be realized. UCLA researchers have successfully integrated three-dimensional micro-optical elements with rotational stages using this process. Figure 17 shows a SEM photograph of a rotatable mirror. The rotatable plate is fabricated on the first polysilicon layer, and the axis and hub are defined on the second polysilicon layer. The indicator on the lower part of the picture, originally pointing at the 0-deg tick, has been rotated counterclockwise by 20 deg after the mirror was assembled, as shown on the picture. A diffraction grating integrated with the rotational stage has been successfully demonstrated using the same technology, as shown in Fig. 17.

4 Potential Applications

In this section we review recent developments and achievements in both micro-optics and MEM and introduce several attractive MOEM devices that have recently been proposed and are being developed at different laboratories. These optical subsystems have capabilities that enable complete integration on a single chip.

4.1 *3-D Tunable Fabry-Perot Etalon*

Tunable Fabry-Perot (FP) etalons are very useful for wavelength-division-multiplexed (WDM) optical communications, optical sensing, and spectral analysis applications. There has been a great deal of interest in applying the micromachining technology to realize compact tunable FP etalons, since most FP etalons are tuned mechanically. Many micromachined FP etalons have been demonstrated, including a vertical single-crystal bulk micromachined Si resonator created by deep dry etching,[15] a surface-micromachined membrane on Si,[16] and epitaxially grown GaAs/AlGaAs cantilevers.[17] However, most of the surface-micromachined filters lie on the surface of the substrate, and cannot be integrated with other micro-optical elements on the same chip. Here, we demonstrate a novel three-dimensional tunable filter implemented on a surface-micromachined free-space micro-optical bench (FS-MOB).[18,19] It can be readily integrated with other micro-optical elements (e.g., collimating and focusing lenses, or cascaded tunable filters for WDM demultiplexers) or fiber-alignment V grooves. Both parallel-plate FP etalons and solid FP etalons have been realized using FS-MOB technology.

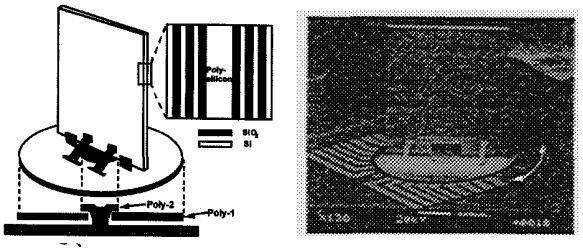

Fig. 18 The schematic and SEM of the tunable solid Fabry-Perot etalon.

A schematic drawing and a SEM micrograph of a solid FP etalon are shown in Figs. 18(a) and 18(b), respectively. The etalon is fabricated by the three-polysilicon layer surface-micromachining technique. The microhinge allows the etalon to be folded into three-dimensional structures after fabrication. The etalon is integrated with a rotation stage for angle tuning of the transmission wavelength. Both surfaces of the polysilicon etalon plate are coated with three pairs of quarter-wavelength SiO_2/Si dielectric layers to increase their reflectivity. The transmission wavelength versus the rotation angle of the etalon is shown in Fig. 19(a). A very broad tuning range of 58.5 nm is obtained when the etalon is rotated by 70 deg. The experimental data agrees very well with a theoretical analysis using the transmission-matrix approach. Figure 19(b) shows the transmission spectrum of the etalon at 50-deg rotation. The finesse of the etalon is measured to be 11, currently limited by the scattering loss due to the granular surface of the polysilicon plate. The finesse could be improved by using parallel-plate FP etalons and smoothing the surface of the polysilicon plates using chemical-mechanical polishing.

4.2 *FDDI Optical Bypass Switch*

The surface-micromachining technique has also been used to demonstrate a single-chip 2×2 optical bypass switch for FDDI (fiber data distribution interface) local area networks. The bypass switch is used in FDDI fiber ring networks to bypass failed computer nodes and enhance network reliability (Fig. 20). It is also useful for reconfigurable optical fiber networks. Free-space optomechanical switches offer several advantages over conventional waveguide switches. Very low insertion loss and small cross talk can be achieved by the free-space approach. In addition, no standby power is required after the switch is reconfigured. Si bulk-micromachining and wafer-bonding techniques

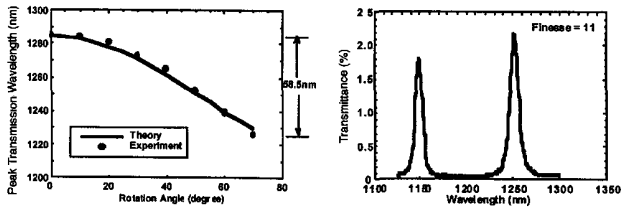

Fig. 19 The wavelength tuning range and the transmission spectrum of the tunable filter.

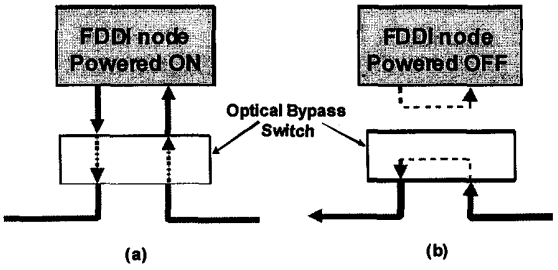

Fig. 20 Schematic diagrams of (a) normal operation and (b) bypass state of the FDDI optical bypass switch.

have been used to implement free-space optomechanical switches.[20] However, monolithic integration is difficult, and substantial assembly is still required. Here, we propose to use the surface-micromachining technology to monolithically integrate the free-space micro-optical switch with microactuators and fiber optic alignment guides.[21] They can be made compact and lightweight, and are potentially integrable with optical sources/detectors and controlling electronics. Moreover, since the switch is made by a photolithographic process, the optical elements can be prealigned during the layout of the photomasks. The assembly and packaging cost can also be reduced.

The switch consists of a three-dimensional movable mirror and four optical fiber guiding rails, as shown in Fig. 21. Four multimode fibers are arranged in a "cross" configuration, with a movable micromirror placed at the center. The switch operates in two states: CROSS and BAR. When the mirror/sliding plate is moved away from the fibers (the center), the fibers along the same diagonal directions are allowed to communicate with each other. This is defined as the CROSS state. In the BAR state, the mirror/sliding plate is slid into the center and the light signal is reflected to the orthogonal fiber. Since no bulk optical lenses are used, the spacing between fiber tips is minimized to reduce optical diffraction loss. Alternatively, integrated out-of-plane refractive microlenses can be used to further reduce the diffraction loss. The movable micromirror consists of a gold-coated out-of-plane polysilicon plate integrated on a sliding plate. The fabrication processes have been described earlier. Figure 22 shows the SEM micrograph of the switch. Top-view photographs of the switch in CROSS and BAR states are shown in Figs. 23(a) and 23(b), respectively.

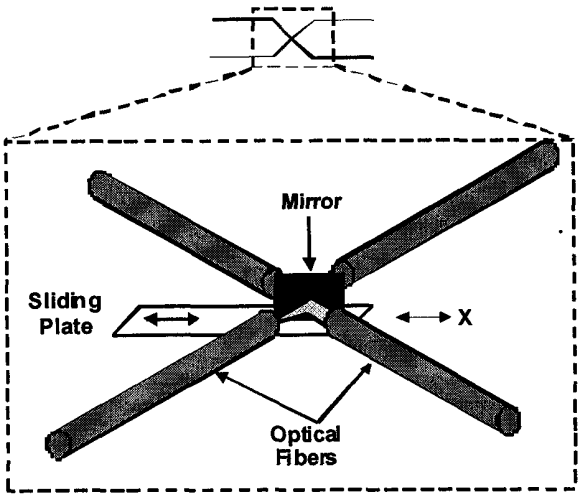

Fig. 21 Schematic diagram of the surface-micromachined FDDI optical bypass switch.

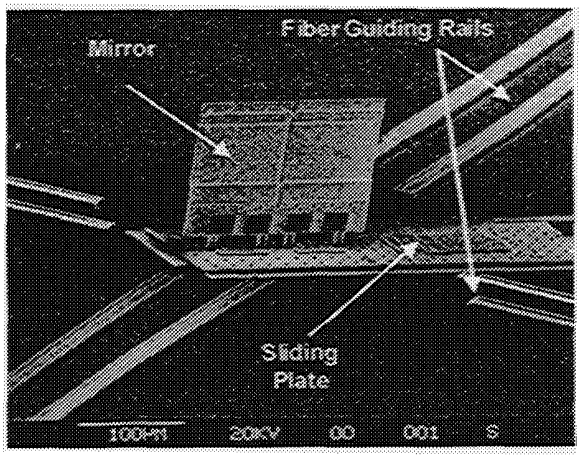

Fig. 22 The SEM of the three-dimensional mirror sitting on a sliding plate.

The optical performance of the optical switch is characterized by attaching multimode fibers to the guiding rails of the optical fibers. The insertion loss of the switch for both operating states has been measured with an LED source operating at 1.3-μm wavelength. The total insertion loss of the switch has been measured to be 2.8 dB for the CROSS state and 3.1 dB for the BAR state. From these two measurements, the reflectivity of the mirror is estimated to be 93%. The cross talk between two states is measured to be 26.1 dB. The theoretical coupling loss between multimode fibers was estimated to be 1 dB for fiber-to-fiber spacing of 125 μm, and 0.45 dB for fiber-to-fiber spacing of 50 μm.[22] The excess loss measured here includes the Fresnel loss of the fiber ($\approx$0.34 dB) and possible misalignment of the fibers. Recently, the insertion losses have been reduced to 1.4 and 1.9 dB, respectively, with an improved design. The diffraction loss is reduced by using lensed fibers for both input and output fibers. Micromachined integrable lenses, antireflection-coated fibers, and a smoother mirror (by chemical mechanical polishing) can be used to further improve the performance of the switch.

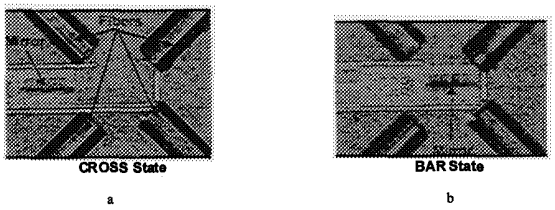

Fig. 23 The top-view photographs of the switch in (a) CROSS state and (b) BAR state.

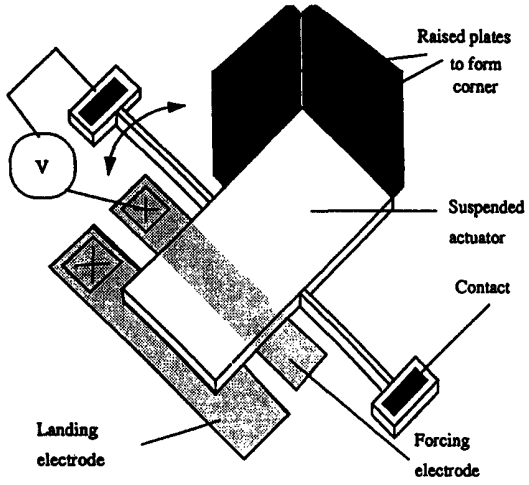

Fig. 24 Schematic diagram of the top view of the corner cube reflector.

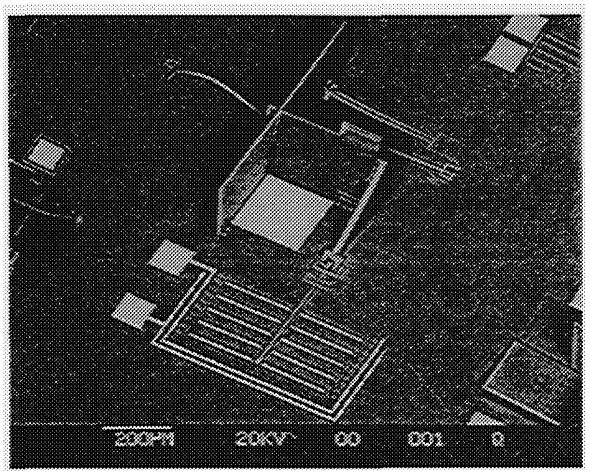

Fig. 25 A corner cube device fabricated using MUMPs process.

4.3 *MEM Corner Cube Reflector*

Micromachined corner cube reflectors (CCRs) fabricated at UCLA have demonstrated the concept of transmitting data digitally by modulating reflected light intensity. CCRs ranging in size from 100 to 200 μm have been built using hinged polysilicon plates. The reflectivity of the polysilicon has been measured to be 24%, and the total reflected power from the corner cube has been measured to be between 1 to 2% of the incident power. The orthogonality between plates is within roughly 8 mrad. Reflection from individual polysilicon plates has been modulated using electrostatic actuation with an applied voltage as low as 8 V.

CCRs have been used in optical systems mainly because, unlike other optical components, they are not critically sensitive to misalignment. A beam of light that hits a defined active area in the concave side of a three-sided orthogonal corner will be reflected back along the axis of arrival to the source. Rays that hit outside this active area do not exit parallel to themselves and therefore do not contribute to the reflected beam. If the orthogonality of the corner cube is disturbed, then the impinging light will not be reflected back to the source. Hence, the intensity of the reflected light can be modulated by small motions of one or more sides of the corner cube. This light modulation can be used to transmit data from the corner cube to the light source with very little power used by the corner cube.

A schematic diagram of the top view of a CCR is shown in Fig. 24. The device is designed using Multi-User MEMS Processes (MUMPs). Each corner cube is made of four 100- to 200-μm-square polysilicon plates rotated out of the surface of the wafer using microfabricated polysilicon hinges as described in Ref. 10, and a long plate suspended by 100- to 200-μm-long thin beams on either side. Two of the rotated plates form the right-angled corner while the remaining two plates serve as supports and orthogonal aligners for setting up the device as a CCR. The long suspended plate also functions as an integral torsional deflection actuator. This plate is actuated electrostatically to deflect the light, thus modulating the reflected intensity. Beneath this plate are two electrodes. One is the landing electrode at the end of the plate, and the other is the forcing electrode. Figure 25 shows a complete processed corner cube device set up for CCR measurements.

To use the corner cube concept as a communication link, the system consists of a number of remote units and one or more base stations. Each remote unit contains a sensor, electronics, a corner cube, a photodiode and a power source. The sensor can be customized for each application. The base station contains a laser source and a photosensor to detect the signal reflected from the corner cube. When the photodiode detects a coded signal from an interrogating laser, the electronic system amplifies, conditions, and digitizes the output from the sensor and feeds the data into a shift register, which starts to output the signal one bit at a time in the form of a voltage that actuates the CCR. A photodetector, placed near the source, will then detect the data transmitted and demodulate them to give the inquirer a digital readout of the sensor output. In a more advanced system, a control system can be integrated so that the base station may send instructions to the remote sensor.

A corner cube sensor as described here has several advantages. Because of its miniature size, the actuation process requires very little power. Thus, the remote unit needs only to have a low-power supply residing within it. A CMOS electronics system can be integrated on chip. This capability, together with the low power consumption, makes the remote unit completely autonomous. In the communication process, the detector does not have to hunt for the reflected signals. As long as it is placed very close to the source, it is guaranteed to receive the transmission. This provides an intrinsically secure communication channel, since competing receivers will not be able to tap into the communication process.

4.4 *Digital Video Using DMDs*

Digital video technology is becoming increasingly important in a networked society and is opening a new technology direction for low-cost projection displays. The natural interface to digital video is a digital display. A digital display accepts electrical bits at its input and converts them into optical bits at the output. The digital-to-analog pro-

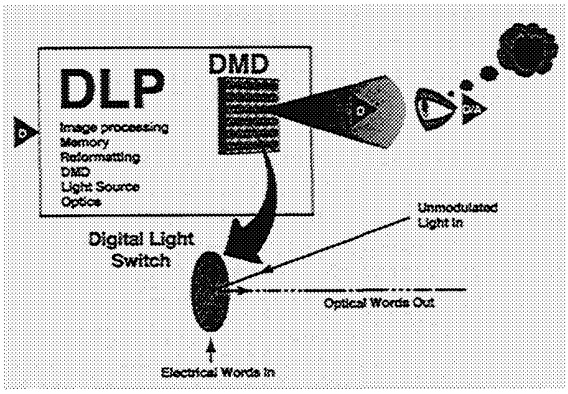

Fig. 26 Digital light-processing system.

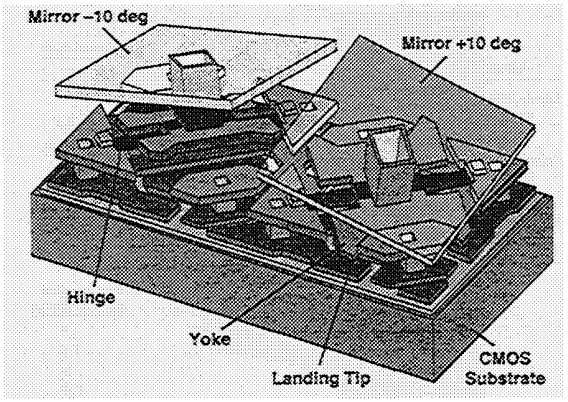

Fig. 27 Two DMD pixels, where mirror is shown transparent and rotated.

cessing function is performed in the mind of the observer. Texas Instruments has developed such a display with its recent market introduction of the Digital Light Processing™ (DLP™) projection display. DLP technology is based on the Digital Micromirror Device™ (DMD), a MEMS array of semiconductor-based digital light switches. The DMD switching array precisely controls a light source for projection display and digital printing applications. Here we present an overview of DLP technology along with architecture, projection operation, and new advances in DMD development.[24–29]

The growth of the global networked society is being driven by the degree to which a common "digital language" is spoken. Digital video technology has become increasingly important to this networked society because of three characteristics: (1) the ease of manipulation of bits for purposes of reducing bandwidth (compression) and for mixing audio, text, graphics, and video (multimedia); (2) the fidelity of digital transmission [e.g., from a direct broadcast satellite (DBS)], digital storage and playback [e.g., with a digital versatile disc (DVD)]; and (3) the possibility of limitless reproduction without degradation.

Figure 26 shows such a digital display based on the Digital Light Processing production display. DLP is based on a MEMS device known as the *digital micromirror device*. Invented in 1987 at Texas Instruments, the DMD is an array of fast, reflective digital light switches. It can be combined with image processing, memory, a light source, and optics to form a DLP system capable of projecting large, bright, seamless, high-contrast color images with better color fidelity and consistency than current displays. DLP systems can also be configured to project images for the production of continuous-tone, near-photographic-quality printing. Numerous publications and presentations have been made on all aspects of DLP and DMD technology, including DLP projection displays.

The DMD light switch (Fig. 27) is a MEMS structure that is fabricated by CMOS-like processes over a CMOS memory. Each light switch has an aluminum mirror, 16 μm square, that can reflect light in one of two directions depending on the state of the underlying memory cell. With the memory cell in the (1) state, the mirror switches to +10 deg. With the memory cell in the (0) state, the mirror switches to −10 deg. On combining the DMD with a suitable light source and projection optics (Fig. 28), the mirror reflects incident light either into or out of the pupil of the projection lens. Thus, the (1) state of the mirror appears bright and the (0) state of the mirror appears dark, and the gray scale is achieved by binary pulse-width modulation of the incident light. Color is achieved by using color filters, either stationary or rotating, in combination with one, two, or three DMD chips.

This mirror structure has been migrated to the 848×600 (SVGA) pixel DMD, and contrast ratios from both front and rear projection systems based on such mirrors routinely exceed 100 :1. We believe this performance will enable the creation of commercially viable systems. With a between-mirrors gap of 1.0 μm, current DMDs with this mirror structure have a fill factor of 89%. The technology is expected to achieve a 0.8-μm between-mirrors gap

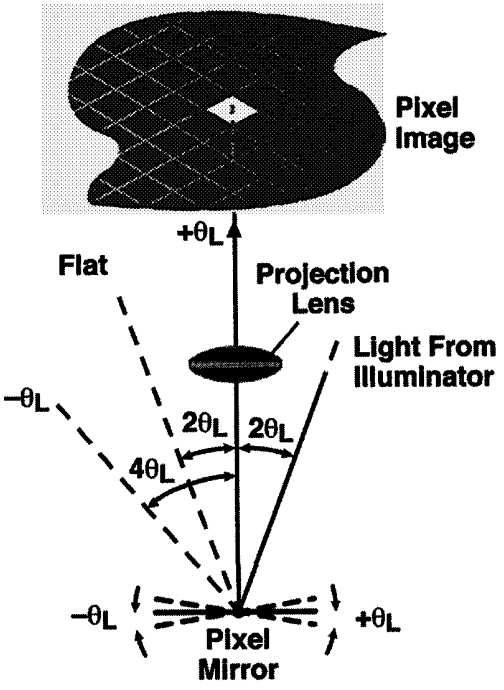

Fig. 28 Optical switching principle of DMD.

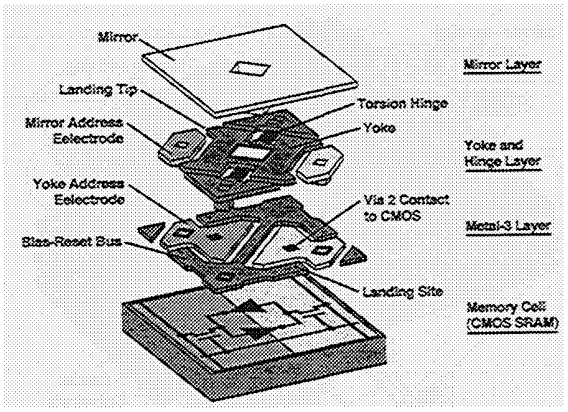

Fig. 29 DMD pixel: exploded view.

that will result in an ultimate fill factor of 91%. Higher contrast ratios can be achieved by limiting the aperture of the projection lens, thus discriminating preferentially in favor of reflected rather than diffracted light, but the system throughput is reduced. Such trade-offs may be justified in nondisplay imaging applications where wider dynamic ranges are required. Contrast ratios exceeding 400 :1 have been observed in such systems.

The DMD pixel is a monolithically integrated MEMS superstructure cell fabricated over a CMOS SRAM cell (Fig. 29). An organic sacrificial layer is plasma-etched to produce air gaps between the metal layers of the superstructure. The air gaps free the structure to rotate about two compliant torsion hinges. The mirror is rigidly connected to an underlying yoke. The yoke in turn is connected by two thin, mechanically compliant torsion hinges to support posts that are attached to the underlying substrate.

Electrostatic fields are developed between the underlying memory cell and the yoke and mirror, creating an electrostatic torque. This torque works against the restoring torque of the hinges to produce mirror rotation in the positive or negative direction. The mirror and yoke rotate until the yoke comes to rest (or lands) against mechanical stops that are at the same potential as the yoke. Because geometry determines the rotation angle, as opposed to a balance of electrostatic torques as in earlier TI devices, the rotation angle is precisely determined. The address electrodes for the mirror and the yoke are connected to the complementary sides of the underlying SRAM cell. The yoke and mirror are connected to a bias bus fabricated at the metal-3 layer. The bias bus interconnects the yoke and mirrors of each pixel to a bond pad at the chip perimeter. An off-chip driver supplies the bias waveform necessary for proper digital operation.

Recent reports from Texas Instruments indicate that a higher-resolution 1280×1024 (SXGA) DMD has been fabricated. While challenges to the fabrication of such high-resolution DMDs remain, these devices have potential use for commercial display applications.

4.5 *Optical Scanners*

A broad spectrum of researchers and innovators from fields such as laser imaging, factory automation, and information handling have made significant contributions to optical scanning. The technology serves such diverse disciplines as printing, graphic arts, image digitizing, quality inspection, bar-code reading, confocal microscopy, data storage, precision pattern generation, display, surveillance, and medical imaging.[31]

Present optical scanners are generally based on oscillatory or galvanometric systems. A galvanometric scanner is electrically steerable to direct a reflected beam onto a target, whereas an oscillatory scanner works at the mechanical resonance of a mirror mount, which typically limits the scan frequency. These mechanisms are usually heavy and expensive, and have poor reliability. The need for low-cost, highly reliable, miniaturized, lightweight optical scanners for both commercial and military applications has been growing during the past decade.

Several micromachined and miniaturized systems are being developed. Rockwell Science Center has developed two kinds of optical scanners. The first kind is a miniature microlens scanner that is a 2-D system driven by piezoelectric actuators to produce addressable points in space. The second kind is a 1-D scanner that covers all points in a linear scan. In the following we present short reviews of a 2-D microlens scanner and a 1-D MEM optical scanner that were developed at the Rockwell Science Center.

4.5.1 *2-D microlens scanner*

A 2-D optical scanner has been developed at Rockwell to modulate the direction of a laser signal. Applications include beam-steering components of laser radar and optical communication systems. Conventional methods that use bulk optical components can result in systems that are too heavy and are not desirable for applications that require rapid optical beam steering, low rotational and translational inertia, and small component displacements. Microlens beam-steering systems fulfill these requirements, achieving a field of view of more than 10 deg with only a fraction of a millimeter of component translation.

The microlens beam-steering device design presented here is based on dithering two complementary (positive and negative) microlens arrays. When the two microlenses are translated relative to each other in the plane parallel to their surfaces, a light beam can be scanned to produce a two-dimensional array of spots. We have demonstrated a miniaturized module consisting of a pair of 6-mm-aperture binary-optics microlens arrays designed for HeNe laser operation. The system can scan the laser beam at rates of 200 Hz or greater. The microlens arrays are optically flat with surface variations on the order of one optical wavelength, permitting separation distances of several microns. Individual lenslet sizes can be in the range of 100 to 200 μm, resulting in maximum translation of similar magnitude. Reducing both the inertia and the travel of the lens system makes the device suitable for agile beam steering.

The microlens arrays were fabricated out of fused quartz using contact lithography and reactive-ion etching. The microlens chips were sawed from a 0.4-mm-thick wafer in squares 10 mm on a side. Each array is driven by a piezoelectric actuator, the two arrays being driven in orthogonal directions. The ultimate module field of view of 10 deg is achieved by translating the array by one-half of a lenslet diameter, which is ± 100 μm.

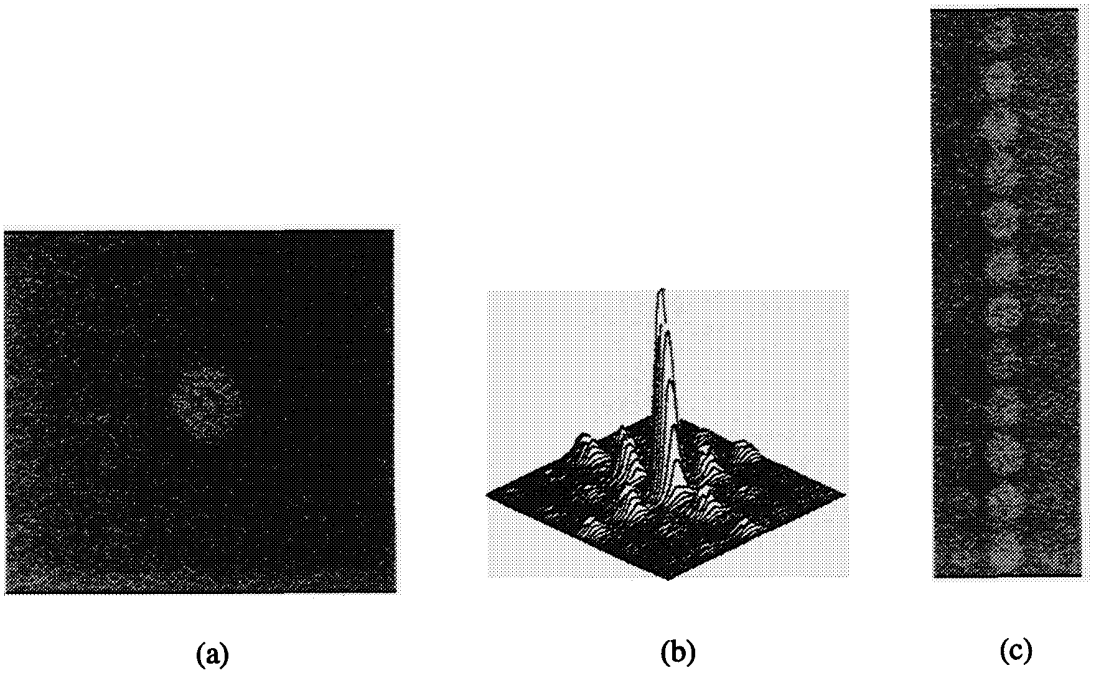

Fig. 30 Characteristic of 2-D microlens scanner developed by Rockwell.

Optical testing was performed on the beam-steering module. The center lobe contains most of the beam energy. The rest of the energy is distributed among the neighboring addressable points. A computerized test bed with a customized digital-to-analog converter board was used to generate drive signals for the scan actuators. Programmable patterns of test signals were output to the piezoelectric transducers to control the beam angle in two dimensions. For more details of scanner operation, refer to Ref. 30.

The characteristics of the 2-D scanner are shown in Fig. 30. Figure 30(a) is a photograph of the scanner output when the beam is stationary. Figure 30(b) is a plot of point-spread-function measurements, which agree with visual observation. Figure 30(c) is the result of a linear scan by removing the x-direction signal and scanning only in the y-direction.

The resulting patterns showed, as predicted, very uniform and well-aligned spots where the majority of the energy is diffracted into a single peak, with lesser amounts into neighboring peaks. The scanner was demonstrated up to a rate of 300 Hz. Operation above 1 kHz is possible with appropriate damping of mechanical resonances. A random point steering was tested experimentally by programming our computerized test bed. The pointing was randomly designed inside an array of 13×13 addressable points. Switching between two points took less than 5 ms.

Rockwell has developed a miniaturized package for a microlens scanner. MEM actuators can be used to reduce the size of this laser scanner package, possibly by two orders of magnitude. Using this approach, we expect to reduce the size of the optical scanner to less than 1 cm^3.

4.5.2 *MEM optical scanner*

Recent advances in micro-optics component development[5] and micro-opto-electro-mechanical (MOEM) systems[9] open a new avenue for miniaturization. We are investigating development of a MOEM scanner engine with a bimorph actuator producing the scanning. Significant microscanning technology innovations, which are highly promising for the future of bimorph optical scanners, are being investigated at Rockwell Science Center. This work is based on our experience in micro-optics, materials development,[32] MEM actuators,[33] and finite-element modeling (FEM).[34]

Issues under consideration are scan angle, driving voltage, structural stability, process compatibility, device size, and mirror flatness. Some are already optimized, and some are yet to be improved. The scan angle is > 20 deg, and the driving voltage is less than 2 V. The structural stability is sufficient at this point, but will require some design changes in the future. The fabrication and assembly processes are CMOS-compatible, and the device size is appropriate. The flatness of the mirror is on the order of a wavelength. These issues contribute to the manufacturability of a device meeting many of the commercial specifications given for different applications.

We have designed a 1-D optical scanner to have a scan-angle range of about 10 to 20 deg. The scanner consists of two main components—an actuator and a mirror on top of a silicon cantilever beam. One reason for using single-crystal silicon instead of another thin-film material is to have higher yield, easier handling, and higher reliability. This is possible due to silicon's relatively high Young's modulus and yield strength. The beam dimensions are typi-

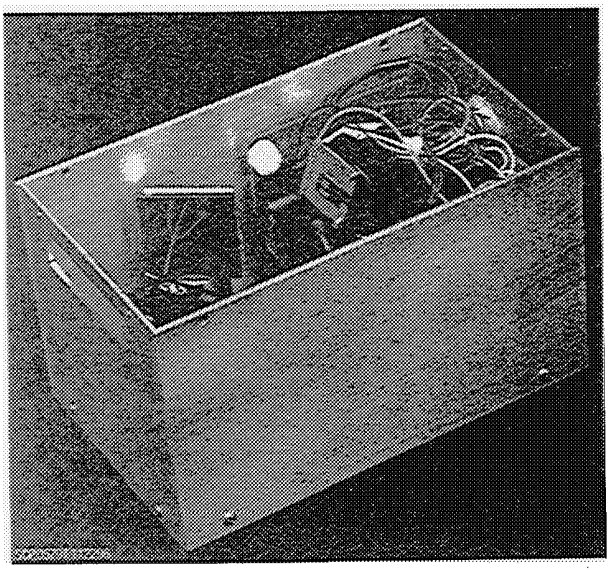

Fig. 31 A photograph of the optical-scanner test bed, showing electrical and optical components including the scanner chip.

cally 6 mm in length, 3 mm in width, and 10 μm in thickness. With the mirror area given for a certain application, an optimal beam thickness is determined to meet commercial operation frequency and scan-angle specifications.

The actuator is placed near the bending axis of a beam that bends through a thermal bimorph effect. This effect is a result of thermal mismatch in two or more layers of film. The beam consists of ZnO covered by two metal layers, which function as top and bottom electrodes. As temperature increases and decreases, the stack of layers expands and contracts accordingly. Depending on the thermal expansion coefficients of the top layers relative to the bottom layers, the beam can bend either upward or downward. The beam is designed to bend upward in a static position and downward with an applied current. This is done by having higher thermal expansion coefficients on the top layers than on the bottom layers, with the right film thicknesses and process temperatures. The bimorph's power efficiency is directly related to the differences in thermal expansion coefficients of the layers.

The area for this actuator takes less than half of the total beam area. The rest of the beam area, at the end of the beam, is dedicated to the mirror. To attain an optical flatness of about a wavelength, the mirror area is designed to be stiffer than the rest of the beam area. This is done by increasing the beam thickness in the mirror area. For certain applications, a layer of metal or a stack of dielectric layers is applied on the mirror area to meet an optical efficiency specification.

Various environmental experiments, including life-cycle tests, have been done to prove the performance integrity of the device over its life expectancy. Scanners have gone through 4×10^9 cycles, operating at 10-deg scan angle. For the purpose of demonstrating an optical scanner, a demonstration module was built to be used as a test bed. A photograph of this module is shown in Fig. 31. For this box, a circularly collimated laser diode is used as a source to eliminate aberrations caused by cylindrical lenses found in many common diode lasers. The scanner chip, mounted on a flat package, is in turn mounted on a rotational stage with two degrees of freedom. This stage is used for fine optical adjustment. The scanned beam exits from an optical window. All electronics and control circuits are packaged inside the box. The ac signal amplitude (0 to 2 V) and operation frequency (60 to 2000 Hz) can be adjusted by two potentiometers accessible from outside the box. The power source is supplied by a small ac adapter. The box dimensions are $5 \times 3 \times 3$ in. Figure 32 shows the module in operation, demonstrating a linear scan of a laser beam.

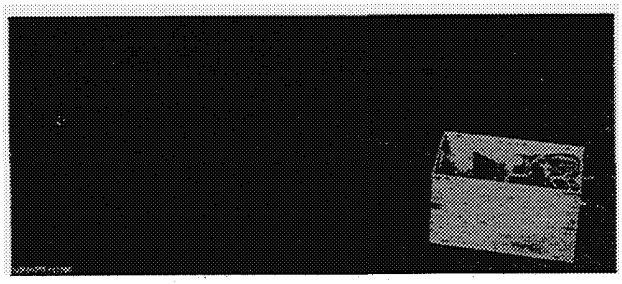

Fig. 32 MEM scan engine demonstrates a linear scan beam.

5 Conclusions

Micro-optics technology, including both diffractive and refractive microlenses, has advanced significantly over the past several years. The use of similar micromachine processes for micro-optics and micromechanics offers the promise for further technology integration and the development of micro-opto-electro-mechanical (MOEM) technology. This enables the incorporation of optical functions into microdevices, resulting in another whole new field for sensors and other microdevices as candidates for on-chip optical processing. Examples include a 3-D tunable Fabry-Perot etalon, an FDDI switch, a corner cube reflector, a digital video display using DMDs, and a 2-D laser scanner. These technologies are expected to gain rapidly in maturity, as they all rely on identical batch processing. We have presented here a few recent developments in this emerging field and have described examples of devices that are being developed. Further significant rapid advances can be expected for on-chip optical processing as researchers recognize the full range of functionality that can be realized using this exciting new technology.

Acknowledgments

The authors gratefully acknowledge the contributions of Dr. Larry Hornbeck at Texas Instruments and Dr. Haluk Sankur at Rockwell Science Center to this paper. This work was supported by Rockwell IR&D and DARPA. Section 4.4 (Digital video using DMDs) has been adapted with permission of the author.[24]

References

1. M. E. Motamedi, W. H. Southwell, R. J. Anderson, W. J. Gunning, and M. Holz, "High speed binary microlens in GaAs," *Proc. SPIE* **1544**, 33–44 (July 1991).
2. M. E. Motamedi, M. P. Griswold, and R. E. Knowlden, "Silicon microlenses for enhanced optical coupling to silicon focal planes," *Proc. SPIE* **1544**, 22–32 (July 1991).
3. M. E. Motamedi, B. Anderson, R. De La Rosa, W. J. Gunning, R. L.

Hall, and M. Khoshnevisan, "Binary optics thin film microlens array," *Proc. SPIE* **1544**, 22–32 (July 1992).
4. H. O. Sankur, R. L. Hall, M. E. Motamedi, W. J. Gunning, and W. E. Tennant, "Fabrication of IR microlens arrays by reactive ion milling," in *Miniature and Micro-optics and Micromechanics, Proc. SPIE* **2687**, 150–155 (1996).
5. H. O. Sankur, M. E. Motamedi, R. Hall, W. Gunning, and M. Khoshnevisan, "Fabrication of refractive microlens arrays," in *Miniature and Micro-optics and Micromechanics, Proc. SPIE* **2383**, 179–183 (1995).
6. M. E. Motamedi, W. E. Tennant, R. Melendes, N. S. Gluck, S. Park, J. M. Arias, J. Bajaj, J. G. Pasko, W. V. McLevige, M. Zandian, R. B. Hall, K. G. Steckbauer, and P. D. Richardson, "FPAs and thin film binary optic microlens integration" (invited paper), in *Miniature and Micro-optics and Micromechanics, Proc. SPIE* **2687**, 70–77 (1996).
7. M. E. Motamedi, W. H. Southwell, H. O. Sankur, R. Melendes, M. Khoshnevisan, F. Durville, X. Wang, C. Liu, R. Rediker, and J. Leger, "Optical transformer and collimater for efficient fiber coupling" (invited paper), *Proc. SPIE* **3008** (1997).
8. M. E. Motamedi, "Merging micro-optics with micromechanics: micro-opto-electro-mechanical (MOEM) devices" (invited paper), *Proc. SPIE* **CR49**, 302–328 (July 1993).
9. M. E. Motamedi, "Micro-opto-electro-mechanical systems" (invited paper), *Opt. Eng.* **33**(11), 3505–3517 (Nov. 1994).
10. K. S. J. Pister, M. W. Judy, S. R. Burgett, and R. S. Fearing, "Microfabricated hinges," *Sensors and Actuators A* **33**, 249–256 (1992).
11. M. C. Wu, L. Y. Lin, S. S. Lee, and K. S. J. Pister, "Micromachined free-space integrated micro-optics," *Sensors and Actuators: A. Physical* **50**(1–2), 127–134 (Dec. 1995).
12. S. S. Lee, L. Y. Lin, and M. C. Wu, "Surface-micromachined free-space fiber optic switches," *Electron. Lett.* **31**(17), 1481–1482 (Aug. 1995).
13. L. Y. Lin, S. S. Lee, K. S. J. Pister, and M. C. Wu, "Three-dimensional micro-Fresnel optical elements fabricated," *Micromachining Technique by Electron. Lett.* **30** (5).
14. L. Y. Lin, S. S. Lee, K. S. J. Pister, and M. C. Wu, "Micro-machined three-dimensional micro-optics for integrated free-space optical system," *IEEE Photon. Technol. Lett.* **6**(12), (Dec. 1994).
15. A. Jazairy, N. C. MacDonald, and Y. H. Lo, "Microelectromechanical Fabry-Perot interferometer," presented at 1995 Optical Society of America Annual Meeting, Sept. 10–15, 1995, Portland, Oregon, Paper WH4.
16. T. T. D. Tran, Y. H. Lo, A. H. Zhu, D. Haronian, and E. Mozdy, "Surface micromachined Fabry-Perot tunable filter," *IEEE Photon. Technol. Lett.* **8**(3), 393–395 (1996).
17. E. C. Vail, M. S. Wu, G. S. Li, L. Eng, and C. J. Chang-Hasnain, "GaAs micromachined widely tunable Fabry-Perot filters," *Electron. Lett.* **31**(3), 228–229 (1995).
18. L. Y. Lin, J. L. Shen, S. S. Lee, M. C. Wu, and A. M. Sergent, "Tunable three-dimensional solid Fabry-Perot etalons fabricated by surface-micromachining," *IEEE Photon. Technol. Lett.* **8**(1), 101–103 (1996).
19. J. L. Shen, L. Y. Lin, S. S. Lee, M. C. Wu, and A. M. Sergent, "Surface-micromachined tunable three-dimensional solid Fabry-Perot etalons with dielectric coatings," *Electron. Lett.* **31**(25), 2172–2173 (1995).
20. M. F. Dautartas, A. M. Benzoni, Y. C. Chen, and G. E. Blonder, "A silicon-based moving-mirror optical switch," *J. Lightwave Technol.* **10**(8) (Aug. 1992).
21. S. S. Lee, L. Y. Lin, and M. C. Wu, "Surface-micromachined free-space fiber optic switches," *Electron. Lett.* **31**(17), 1481–1482 (Aug. 1995).
22. P. Di Vita and U. Rossi, "Evaluation of coupling efficiency in joints between optical fibers," *Alta Frequenza* **XLVII**(7), 414–423 (1978).
23. D. S. Gunawan, Lih-Yuan Lin, and K. S. J. Pister, "Micromachined corner cube reflectors as a communication link," *Sensors and Actuators A* **46–47**, 580–583 (1995).
24. L. J. Hornbeck, "Digital light processing and MEMS: reflecting the digital display needs of the networked society," (invited paper), presented at SPIE/EOS European Symposium on Lasers, Optics, and Vision for Productivity in Manufacturing I, Besancon, France, June 10–14, 1996.
25. R. L. Knipe, "Challenges of a digital micromirror device: modeling and design," presented at SPIE/EOS European Symposium on Lasers, Optics, and Vision for Productivity in Manufacturing, Besancon I, France, June 10–14, 1996.
26. L. J. Hornbeck, "Current status of the digital micromirror device (DMD) for projection television applications" (invited paper), in *International Electron Devices Technical Digest*, pp. 381–384 (1993).
27. J. B. Sampsell, "An overview of the digital micromirror device (DMD) and its application to projection displays," in *1993 SID International Symposium Digest of Technical Papers*, Vol. 24, p. 1012 (1993).
28. C. Tew, "Electronic control of a digital micromirror device for projection displays," in *1994 IEEE Solid-State Circuits Digest of Technical Papers*, Vol. 37, p. 130 (1994).
29. J. Younse, "Mirrors on a chip," *IEEE Spectrum* **30**(11), 27 (Nov. 1993).
30. M. E. Motamedi, A. P. Andrews, W. J. Gunning, and M. Khoshnevisan, "Miniaturized micro-optical scanners" (invited paper), *Opt. Eng.* **33**(11), 3616–3623 (Nov. 1994).
31. G. F. Marshal, "Advances in oscillatory optical scanners," in *Micro-optics Micromechanics and Laser Scanning and Shaping, Proc. SPIE* **2383**, 440–448 (1995).
32. S. Park, M. S. Dadkhah, and M. E. Motamedi, "Characterization of silicon nitride thin film by interferometry and FEA" (abstract), in *Proc. VIII International Congress on Experimental Mechanics*, pp. 7–8, June 10–13 (1996).
33. J. J. Yao and M. F. Chang, "A surface micromachined miniature switch for telecommunications applications with signal frequencies from dc up to 4 GHz," in *Transducers '95*, pp. 384–387 (June 1995).
34. M. S. Dadkhah, D. B. Marshal, and W. L. Morris, "Direct measurement of transformation zone strain in toughened zirconia," *J. Am. Ceramic Soc.* **74**(3), 584–592 (1991).

M. Edward Motamedi: Biography and photograph appear with the special section guest editorial in this issue.

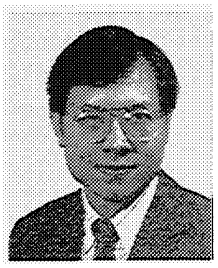

Ming C. Wu received his MS and PhD degrees in electrical engineering from the University of California/Berkeley in 1985 and 1988, respectively. From 1988 to 1992, he was a member of the technical staff at AT&T Bell Labs, where he conducted research in high-speed semiconductor lasers and optoelectronics. In 1993, he joined the faculty of the Electrical Engineering Department of the University of California/Los Angeles as associate professor. His current research interests include micro-opto-electro-mechanical systems, optical MEMS and their applications to free-space integrated optics, ultrafast integrated optoelectronics, semiconductor lasers, and optical interconnects. He has served as general co-chair for the IEEE LEOS Summer Topical Meeting on Optical MEMS and Their Applications in 1996, and general co-chair for the IEEE LEOS Summer Topical Meeting on RF Optoelectronics in 1995. He also served on the program committee of CLEO in 1996 and 1997, IEDM in 1996, and Photonics West in 1997. He was awarded the Packard Foundation Fellow in 1992. He received the Meritorious Conference Paper Award of 1994 GOMAC. He has published over 80 papers in research journals and 110 papers in refereed conferences, contributed to one book chapter, and holds 8 U.S. patents. Dr. Wu is a member of IEEE, American Physical Society, Optical Society of America, URSI, and Eta Kappa Nu.

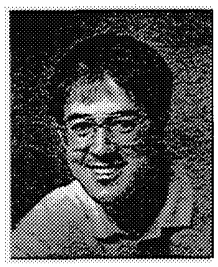

Kristofer S. J. Pister received his BA in applied physics from the University of California/San Diego in 1982, and his MS and PhD in electrical engineering from the University of California/Berkeley (U.C. Berkeley) in 1989 and 1992. In 1992 he became an assistant professor of electrical engineering at the University of California/Los Angeles, where he developed three graduate-level courses in micro-electro-mechanical systems: MEMS device physics and fabrication, MEMS system design, and CAD for MEMS. In 1996 he joined the faculty of Electrical Engineering and Computer Sciences at U.C. Berkeley. During the last four years, his primary research interest has been the development and use of standard fabrication technologies, general purpose design paradigms, and software support for MEMS design. Some of the applications of his research include microrobotics, micro-optics, distributed sensor networks, and biomedical instruments. He is an active consultant in the MEMS industry, and has two patents pending on MEMS technology and applications.